 doi:10.20944/preprints201705.0144.v1

Neuroprotective Effect of Anthocyanin Extract from *Lycium ruthenicum* Murray in $A\beta_{1-42}$-induced Rat Model of AD

Xueling Wu [a] , Xiaoxiao Li [a], Shuang Liang [a], Yanxia Liu [a], Xueling Dai [a], Qiusheng Zheng [b], Yaxuan Sun [a] *[1]

[a] Beijing Key Laboratory of Bioactive Substances and Functional Foods, Beijing Union University, Beijing 100191, China

[b] Binzhou Medical University, School of Chinese Medicine Integrated with Western Medicine, Yantai 264003, China

Abstract: Alzheimer's disease (AD) is an age-related neurodegenerative disease and is clinically characterized by cognitive impairment, memory loss, and personality disorder. Oligomers of amyloid beta-peptides (Aβ) and enhanced oxidative stress in senile plaques are prevalent pathologic hallmarks of AD. In this study, we detected the behavioral performance of *Lycium ruthenicum* Murray anthocyanin (LRA) -treated rats using the Morris water maze test and then investigated the effect of LRA on oxidative damage, neuronal apoptosis, and inflammatory response induced by $A\beta_{1-42}$. Our results showed that LRA treatment markedly ameliorated the behavioral performance of $A\beta_{1-42}$-induced rats and reduced the level of malondialdehyde, formation of protein carbonyl, and 8-hydroxy-2'-deoxygua-nosine. Furthermore, LRA also inhibited activated astrocytes and neuroinflammation via suppression of glial fibrillary acidic protein and tumor necrosis factor-alpha in the hippocampus of $A\beta_{1-42}$-treated rat brain. These data suggest that LRA could be a potential anti-oxidant and anti-neuroinflammatory agent for the treatment of AD.

Keywords: Alzheimer's disease (AD); amyloid-β_{1-42}($A\beta_{1-42}$); *Lycium ruthenicum* Murray (LRA); neuroprotective effect

1. Introduction

Alzheimer's disease (AD) is an age-related neurodegenerative disease affecting a large and continuously increasing population of 65 years of age or older. 46.8 million people suffered from this disease have been reported until 2015, and this number was expected to grow to nearly 131.5 million by 2050 [1, 2]. AD is pathologically characterized by neuronal and synaptic losses, intracellular neurofibrillar tangles (NFTs) containing hyperphosphorylated tau protein, and senile plaques (SPs) formed from numerous extracellular amyloid beta-peptides (Aβs) generated by the proteolytic cleavage of amyloid precursor protein (APP) [3]. APP could be successively

*Corresponding author. Tel: +86 010 62004604.e-mail: sunxx@buu.edu.cn (Yaxuan Sun) ;

Preprints (www.preprints.org) | NOT PEER-REVIEWED | Posted: 19 May 2017 doi:10.20944/preprints201705.0144.v1

cleaved by β- and γ-secretase complexes resulting in peptides composed of 38–43 amino acids named Aβ [4]. Previous studies have established the $A\beta_{1-42}$ as an important factor in determining the fibrillogenesis, toxicity, and pathological distribution of Aβ [5]. Researchers believe that Aβ aggregation in the brain triggers the pathogenesis of AD, though the precise mechanism of AD remains unknown [6].

Aβ deposition promotes production of reactive oxygen species (ROS) via inflammatory response that eventually leads to apoptosis [7, 8, 9]. Oxidative stress is the imbalance between anti-oxidant level and ROS overproduction, thereby inducing potential brain damage [10]. The production of ROS can lead to lipids, proteins, and DNA/RNA damage and modifications [11], thus resulting in the generation of several potent reactive molecules, such as malondialdehyde (MDA), protein carbonyl (PC), and 8- hydroxydeoxyguanosine (8-OHdG) [12, 13]. As the main source of ROS and major target of oxidative damage, progressive impairment of mitochondrial function has been implicated in AD [14]. Impaired mitochondrial function has been associated with activation of mitochondrial apoptotic pathways. These pathways include pro-apoptotic protein Bax, followed by the release of cytochrome C into cytosol and the activation of caspases, such as caspase-9 and caspase-3 [15]. Other sources of ROS in brain are from microglia and astrocytes when activated and also in reactions catalyzed by redox active metal ions such as copper and iron [16]. These cells may stimulate the reproduction of several proinflammatory cytokines, including tumor necrosis factor α (TNF-α) and glial fibrillary acidic protein (GFAP), which may contribute to neuronal degeneration and cell death [17]. Although many researches have been directed to AD treatment, there is still no promising treatment for the disease. Currently, much attention has been focused on the potential of using natural herbs as auxiliary strategies for treating or preventing AD.

Lycium ruthenicum Murray (LRA) is an important medicinal plant and well recognized for its potential health benefits. Most of the health-promoting properties of LRA are mainly from anthocyanins, which are a group of compounds structurally belonging to the natural products of flavonoids and responsible for the blue color of plants (Fig. 1) [18]. Anthocyanins not only exhibit potent anti-oxidative, anti-inflammatory, and anti-carcinogenic activities, but also exert cardioprotective and neuroprotective effects [17, 19, 20]. Growing evidence has shown the beneficial effects of anthocyanins on memory and cognition in neurodegenerative diseases, including AD[21, 22]. In this study, we studied the neuroprotection and potential mechanism of LRA against $A\beta_{1–42}$-induced oxidative stress, neuroinflammation, and memory impairment in rat model of AD.

2. Results

2.1. Effects of LRA on rat performance in the Morris water maze test

Preprints (www.preprints.org) | NOT PEER-REVIEWED | Posted: 19 May 2017 doi:10.20944/preprints201705.0144.v1

The effect of LRA on spatial learning and memory in $A\beta_{1-42}$-induced AD rats was analyzed by Morris water maze test. In the training test, Morris water maze (4 d, 3 trails/d) was used, and data analyses were conducted by two-way ANOVA. The data showed statistically significant difference among the groups ($F(5, 264) = 114.915$, $P<0.01$); highly significant difference among the days ($F(3, 264) =970.485$, $P<0.01$); and significant effect of interaction between groups and days ($F(15, 264) = 5.798$; $P<0.01$). The latency in finding the platform decreased gradually in all groups (Fig.2A). However, the $A\beta_{1-42}$-treated rats showed longer latency to find the platform than those of the control group. The rats treated with LRA (20, 40, and 80 mg/kg) located to the hidden platform more efficiently than the model group. Meanwhile, the latency to platform was revealed during the probe test (Fig. 2B). The $A\beta_{1-42}$-injected rats exhibited pronouncedly longer escape latency than the control group ($P < 0.01$). The huperzine-A group (0.2 mg/kg) and LRA-treated groups (20, 40, and 80 mg/kg) significantly ($P < 0.01$) shortened the latency to the platform during the probe test compared with those of the model group. Meanwhile, the number of platform crossings was considered as the search frequency in the probe test (Fig. 2C). Compared with the model group, the search frequency in the huperzine-A group (0.2 mg/kg) and LRA-treated groups (20, 40, and 80 mg/kg) were obviously increased ($P < 0.01$). This result showed that the impaired spatial learning and memory ability in $A\beta_{1-42}$-induced AD rats, and LRA treatment could ameliorate the memory impairment.

2.2. Effects of LRA on the levels of T-SOD, CAT, GSH, PC, and MDA

T-SOD, CAT, and GSH are three predominant antioxidants that protect cells against free radicals and subsequent oxidative damage. MDA and PC are the end products of lipid peroxidation and protein oxidation respectively, which can reflect the extent of oxidative stress. The effects of LRA on the levels of T-SOD, CAT, GSH, MDA, and PC in the hippocampus were analyzed (Table 1). Compared with those observed in the control group, the level of T-SOD, CAT, and GSH was significantly decreased ($P < 0.01$), whereas the levels of MDA and PC was significantly increased ($P < 0.01$) in the model group. However, compared with the model group, the huperzine-A group (0.2 mg/kg) showed obviously increased level of T-SOD, CAT, and GSH ($P < 0.05$, $P < 0.01$, and $P < 0.01$, respectively), and significantly decreased levels of MDA and PC ($P < 0.01$). Compared with the model group, the LRA-H group (80 mg/kg) effectively increased ($P < 0.01$) the levels of T-SOD, CAT, and GSH, and significantly decreased ($P < 0.0$ 1) the generation of MDA and PC. The LRA-M group (40 mg/kg) exhibited significantly increased level of T-SOD, CAT, and GSH ($P < 0.05$, $P < 0.01$, and $P < 0.01$, respectively, vs. the model group) and decreased level of MDA and PC ($P < 0.01$ and $P < 0.05$, respectively, vs. the model group). The LRA-L group (20 mg/kg) effectively increased the level of CAT and GSH ($P < 0.05$ vs. the model group) and significantly decreased the level of MDA ($P < 0.01$ vs. the model group).

Preprints (www.preprints.org) | NOT PEER-REVIEWED | Posted: 19 May 2017 doi:10.20944/preprints201705.0144.v1

2.3. Effects of LRA on Aβ$_{1–42}$-induced hippocampal neuronal morphology change

To investigate the effect of LRA on the Aβ$_{1–42}$-induced neuronal morphological change in hippocampus, we performed Nissl and hematoxylin and eosin (H&E) staining analyses. The Nissl staining results for each group are shown in Fig. 3, and H&E staining results are displayed in Fig. 4. In the control group, no histopathological changes were observed in the CA1 region of hippocampus. However, neuronal damages, such as nuclear pyknosis and indefinable borders between nuclei and cytoplasm, were observed in the pyramidal neurons of the model group rats. Interestingly, neurons from the LRA-treated groups significantly reversed the Aβ$_{1–42}$-induced CA1 neuronal damage. This phenomenon was particularly evident with doses of 40 and 80 mg/kg.

2.4. Effects of LRA on Aβ$_{1–42}$-induced hippocampal neuronal apoptosis

TUNEL assay was used to investigate the neuronal apoptosis in the CA1 region of hippocampus. Representative photographs of TUNEL staining in the hippocampus were presented in Fig. 5, and the quantification of TUNEL labeling in each group was shown in Fig. 5G. TUNEL-positive apoptotic cells of the control group were less than those in the model group ($P < 0.01$). Moreover, the huperzine-A and LRA-treated groups (20, 40, and 80 mg/kg) significantly decreased the number of apoptotic cells ($P<0.01$, $P<0.01$, $P<0.01$, and $P<0.05$ vs. the model group).

2.5. Effects of LRA on 8-OHdG levels

8-OHdG is a sensitive marker of DNA damage. The effect of LRA on the level of 8-OHdG in the hippocampus was investigated. As shown in Fig. 6, the model group showed significantly increased ($P < 0.01$) levels of 8-OHdG compared with those of control group. However, this increase was suppressed by treatment with huperzine-A, LRA-H, LRA-M, and LRA-L.

2.6. Effects of LRA on caspase-3 levels

caspase-3 is a major mediator of both apoptotic and necrotic cell death. The effect of LRA on the level of caspase-3 in the hippocampus was also investigated. As shown in Fig. 7, the model group showed significantly increased ($P < 0.01$) levels of caspase-3 compared with those of control group. However, compared with the model group, this increase was suppressed by treatment with huperzine-A, LRA-H, LRA-M, and LRA-L group (except for LRA-L, all at $P <0.01$).

2.7. Effects of LRA on GFAP and TNF-α levels

GFAP and TNF-α are expressed in the astrocytes and microglia respectively, which are involved in the inflammatory reactions. Fig. 8 and Fig. 9 reveal the effect of LRA on the level of GFAP and TNF-α in the CA1 region of hippocampus. No significant expression of GFAP and TNF-α was found in the control group. However, the area and intensity of GFAP staining were

Preprints (www.preprints.org) | NOT PEER-REVIEWED | Posted: 19 May 2017 doi:10.20944/preprints201705.0144.v1

significantly increased in the model group ($P < 0.01$), though this increase was markedly reversed in all of the LRA-treated groups ($P < 0.01$). Meanwhile, the level of TNF-α was also significantly increased in the model group ($P < 0.01$). Notably, the huperzine-A (0.2 mg/kg) and LRA-treated (20, 40, and 80 mg/kg) groups significantly decreased the expression of TNF-α compared with the model group ($P < 0.01$).

3. Discussion

Aβ is a chief component of SP and plays a pivotal role in the pathogenesis and progression of AD [23]. Aβ can cause cell toxicity by inducing oxidative stress derived from an imbalance between the generation and detoxification of ROS [24]. The overproduction of ROS can promote the oxidation of major biomolecules, including protein, lipids, DNA, and RNA [25]. Our results revealed that LRA at the dose of 40 and 80 mg/kg enhanced the levels of GSH, CAT, and T-SOD, and decreased the levels of MDA, PC, and 8-OHdG in the Aβ-induced rat model of AD. Previous studies revealed that the dysfunctional mitochondria are the major sources of ROS generation because of the unavoidable electron exposure and the activation or alteration of many components of the mitochondrial apoptotic pathway including caspase-3, which is linked to tau cleavage and NFT formation [26, 27]. This result agrees with our immunohistochemical staining of caspase-3, which showed that LRA significantly reduced the levels of active caspase-3 in the rat hippocampus.

Other sources of ROS in the brain are microglia and astrocytes that produce these species when activated and induce neuroinflammation. In the pathological state, the activation of astrocytes can activate inflammatory reaction and produce cell inflammatory factors and ROS. This reaction may eventually result in the damage or death of nerve cell and further lead to the pathological process of AD [28]. However, GFAP is the specificity protein and skeletal building block of astrocytes and can thus be used as a sign of astrocyte proliferation reaction after brain injury [29]. Moreover, microglia are activated by the stimulation of Aβ; they also induce the synthesis and secretion of proinflammatory factor that can produce neurotoxins and induce neuronal apoptosis, including interleukin 1 beta, interleukin 6, TNF-α, and interferon gamma (IFN-γ) [30]. TNF-α and IFN-γ can exhibit neurotoxicity and reduce the activity of insulin-degrading enzyme that is key to the Aβ degradation enzyme [31]. Hence, TNF-α and IFN-γ can further increase Aβ deposition through this mechanism. Similarly, in this study, LRA treatment (20, 40, and 80 mg/kg) could significantly inhibit elevated expression of TNF-α and decreased level of GFAP.

Anthocyanins exhibit potent anti-oxidant activity that accounts for its anti-inflammatory, anti-carcinogenic, and neuroprotective properties [32, 33]. Current evidence also presents sound basis for exploring the potential of using LRA extracts as an auxiliary strategy for treating and preventing AD [34, 35]. Thus, we utilized an $A\beta_{1-42}$-induced rat model of AD to investigate the neuroprotective role of LRA, which was demonstrated as a potential therapeutic agent against AD. Morris water maze test is widely used in determining the learning and memory ability of

Preprints (www.preprints.org) | NOT PEER-REVIEWED | Posted: 19 May 2017 doi:10.20944/preprints201705.0144.v1

animals [36,37]. Our results indicated that LRA, particularly at higher doses (40 and 80 mg/kg), could significantly ameliorate $A\beta_{1–42}$-induced spatial learning and memory impairment in rats. The mechanism can be attributed to reduced level of ROS and decreased Aβ-induced damage to the brain. This result was in accordance with our Nissl and H&E staining and immunohistochemical staining (TUNEL), which suggest that administration of LRA, especially at doses of 40 or 80 mg/kg, could significantly ameliorate cell loss and neuron injury. Besides, LRA treatment could also reduce the number of $A\beta_{1–42}$-induced apoptotic cells. Therefore, anti-oxidative mechanisms are crucial to the ability of LRA in reducing Aβ-induced hippocampal memory deficits and neurodegeneration.

In summary, our study demonstrated that LRA effectively attenuated oxidative stress, neuroinflammation, and damage-induced memory impairment in $A\beta_{1–42}$-induced AD model. The findings of the present study suggest that LRA is a promising antioxidant and anti-neuroinflammatory agent for AD treatment. However, further studies are required to investigate the possible mechanism of the neuroprotective effect of LRA.

4. Materials and methods

4.1. Materials

Anthocyanins extracted from LRA were provided by the Biochemical Engineering College of Beingjing Union University. $A\beta_{1-42}$ was purchased from GL Biochem Ltd (Shanghai, China). Assay kits of total superoxide dismutase (T-SOD), glutathione (GSH), catalase (CAT), malondialdehyde (MDA) and protein carbonyl (PC) were purchased from Jiancheng Bioengineering Institute (Nanjing, China). The DNA fragmentation detection kit (TUNEL) was obtained from Roche Molecular Biochemicals (Germany). The Nissl and H&E staining solution were purchased from Beyotime Biotechnology Co., Ltd (Beijing China). 3,3’-diaminobenzidine (DAB) substrate kit was purchased from Beijing Zhongshan Biotechnology Co., Ltd (Beijing China). All other common chemicals and reagents were of analytical grade.

4.2. Preparation of $A\beta_{1-42}$ oligomers

$A\beta_{1-42}$ was dissolved into hexafluoroisopropanol (HFIP, Sigma) to achieve a concentration of 1 mM, and vacuum dried to remove residual HFIP. Afterwards, dimethyl sulfoxide (DMSO) was then added to obtain a concentration of 5 mM, after which the phosphate-buffered saline (PBS, pH 7.4) was added to yield a final concentration of 2.5μg/μl. After incubation at 4°C for 24 h, $A\beta_{1-42}$ oligomers was stored at - 80°C until use.

4.3. Animals and Treatment

Sprague-Dawley (SD) male rats [6 weeks old, Weitong Lihua Experimental Animal Central; User License: SCXK (jing) 2012-0001] weighing 180-200 g were housed under a 12 h light/dark cycle at 22±1°C , 55±5% humidity with chow and water *ad libitum*. Rats were randomly divided into six groups as follows: control group (0.01M PBS+ sterile water); model

Preprints (www.preprints.org) | NOT PEER-REVIEWED | Posted: 19 May 2017 doi:10.20944/preprints201705.0144.v1

group ($A\beta_{1-42}$ + sterile water); positive control group ($A\beta_{1-42}$ + 0.2 mg/kg huperine-A); LRA-H treated group ($A\beta_{1-42}$ + 80 mg/kg LRA); LRA-M treated group ($A\beta_{1-42}$ + 40 mg/kg LRA); LRA-L treated group ($A\beta_{1-42}$+20 mg/kg LRA).

4.4. Surgery and administration

The oligomers $A\beta_{1-42}$ (2.5μg/μl) was infused into intra-cerebro-hippocampal CA1 area (5 μL) bilaterally using a Hamilton microsyringe at stereotaxic co-ordinates from bregma (anteroposterior (AP) = 3.3 mm, mediolateral (ML) = ±2.0mm and dorsoventral (DV) = 3.4 mm) under anesthesia (2% sodium pentobarbital, 0.35 ml/100g). After surgery, huperzine-A group (0.2 mg/kg) and LRA-treated groups (20, 40, and 80 mg/kg) were treated orally for 15 d, while the control and model groups were treated with sterile water for 15 d.

4.5. Morris water maze test

After $A\beta_{1-42}$-injection, spatial learning and memory was assessed via Morris water maze. The apparatus of Morris water maze test is mainly composed of circular water tank (145 cm in diameter and 60 cm in height) filled with water (24 ±1 °C) that was made opaque by adding india ink. The tank was randomly divided into four quadrants (northeast, southeast, southwest, and northwest) and an escape platform was placed in the center of any of these quadrants, at a depth of 2 cm below water. Three daily training trials were conducted for four consecutive days. Rats that found the platform were allowed to remain on the platform for 15s. If a rat failed to reach the platform within 90s, it was gently guided to the platform by the experimenter. In test section (after training for 4 consecutive days), probe test was performed and rats were allowed to swim freely for 60 s while removing the platform. For the probe trial, the latencies, and number of platform crossings were calculated. Data was recorded using visual tracking system.

4.6. Tissue processing

After treatment, rats (n = 8 rats/group) were sacrificed and brains were immediately removed. Hippocampi isolated from the brain were frozen in liquid nitrogen and stored at -80 °C until use. The remaining animals from each group (n = 4 rats/group) were perfused transaortically first with 0.1 M PBS followed by 4% paraformaldehyde (pH 7.4) under anesthesia. Afterwards, the brain was then removed and placed in 4% paraformaldehyde. After embedding in a paraffin wax block, 4 μm coronal brain slices were obtained and used for immunohistochemical staining.

4.7. Measurement of T-SOD, GSH, CAT, MDA, and PC levels

Hippocampus tissue samples were homogenized in normal saline. The mixture was centrifuged at 3000r/min for 10 min at 4 °C. The supernatant was collected and used for the experiments. The levels of T-SOD, GSH, CAT, MDA, and PC were measured using commercially available assay kits. All kits were used in accordance with the manufacturer's instructions.

Preprints (www.preprints.org) | NOT PEER-REVIEWED | Posted: 19 May 2017 doi:10.20944/preprints201705.0144.v1

4.8. Nissl (cresyl violet) staining

Brain slices were first dewaxed in xylene for 15 min and then progressively rinsed in 100% alcohol (for 5 min), 90% alcohol (for 2 min), 70% alcohol (for 2 min) and finally distilled water (for 2 min). After that, slices were stained in cresyl violet for 5 min and then washed twice in 90% alcohol and distilled water (every time for seconds), respectively. Slices were dehydrated for 2 min using 95% ethanol, cleared in xylene for another 5 min, and covered with Permount TM Mounting Medium and a cover-slip.

4.9. Hematoxylin and eosin (H&E) staining

The H&E Staining was used to observe the morphology of pyramidal neurons in the CA1 region of hippocampus under a light microscope. The tissue sections were dewaxed in xylene for 10 min and rehydrated using different gradients of ethanol (100%, 90%, and 70%) for 2 min, respectively. Subsequently, tissue sections were stained with hematoxylin staining solution for 10 min, and then stained with eosin staining solution for 1 min. Finally, the sections were dehydrated, cleared, and then covered with cover slip.

4.10. TUNEL assay

The TUNEL reaction preferentially labels DNA strand breaks generated during apoptosis. Those DNA strand breaks can be identified by labeling free 3'-OH termini with modified nucleotides in an enzymatic reaction. Tissue sections (4 µm thick) were washed in xylene and rehydration through a graded series of ethanol (100%, 95%, 85%, and 75%) and then diluted in double distilled water. Tissues were then washed three times for 5 min each using PBS. Proteinase K (20 µg/ml) was then added and incubated at 37°C for 20 minutes, after which tissue was again washed three times (5 min/wash) with PBS. Afterward, slices were treated with 50 µl of TUNEL mixture containing terminal deoxynucleotidyl transferase and deoxynucleotide for 60 min at 37 °C. Subsequently, slices were rinsed with PBS for 3 min and incubated with 50 µl of converter-POD solution for 30 min at 37 °C. Slices were incubated briefly in 50 µl of DAB and then rinsed three times in PBS. Finally, slices were dehydrated, cleared, and cover slipped with mounting medium.

4.11. Immunohistochemical analysis of 8-OHdG, GFAP, and caspase-3

Brain tissue sections were baked for 2 hours at 65°C after 4µm coronal sections were cut using a paraffin wax slicer. Tissue sections were washed in xylene for paraffin removal and were then immersed in graded ethanol solutions (100%, 100%, 95%, and 75%). Sections were rinsed five times for 2 min each using PBS before being placed in an EDTA buffer solution (pH 8.0) and boiled in a pressure-cooker for 2 min. Sections were then rinsed five times for 2 min each using PBS, followed by incubation for 15 min in 3% H_2O_2 solution to remove endogenous peroxidase activity, followed by three rinses in PBS (5 min/rinse). The sections were blocked in 5% goat serum for 10 min and then rinsed five times in PBS (2 min/rinse). Sections were

 doi:10.20944/preprints201705.0144.v1

incubated with antibody (SP Immunohistochemical Staining Kit, Beijing Zhongshan Biotechnology Co., China) overnight at 4°C. After incubation, tissue sections were washed in PBS for 10 min, and incubated with the second antibody for 30 min at 37°C, and rinsed again. Reaction product was visualized with a DAB substrate kit. Finally, sections were dehydrated by step gradient alcohol (form low concentration to high concentration), cleared in xylene, and cover slipped with mounting medium.

4.12. Data analysis

All values were presented as means ± SD. The Morris water maze data were analyzed by two-way analysis of variance (ANOVA) with repeated measures followed by Bonferroni multiple comparison test. When group variances were heterogeneous, we used one-way ANOVA and Bonferroni's post-hoc test. $P < 0.05$ was used to indicate significant differences, and $P < 0.01$ was used to indicate extremely significant differences.

Acknowledgements

This work was supported by grants from the Scientific Research Common Program of Beijing Municipal Commission of Education (SQKM201611417002, SQKM201511417013).We gratefully acknowledge financial support of Scientific Research Project from Facing Characteristic Discipline of Beijing Union Unversity(KYDE40201703).

Author Contributions

All authors named on the manuscript have made a significant contribution to the writing, concept, design, execution, or interpretation of the work represented.

Conflict of interest statement

All authors declare that there are no conflicts of interest.

References

1. Querfurth, H. W.; Laferla, F. M. Alzheimer's disease. *N. Engl. J. Med*. 2010, 362, 329-44.
2. Prince, M.; Wimo, A.; Guerchet, M.; Ali, G. C.; Wu, Y. T.; Prina, M. The global impact of dementia. an analysis of prevalence, incidence, cost and trends. *World alzheimer report 2015*.
3. Joe A.; Ksenia K.; Bondulich, M.; Croft, C. L.; Garwood, C. J.; Chhabra, R. Calpain cleavage and inactivation of the sodium calcium exchanger-3 occur downstream of aβ in alzheimer's disease. *Aging Cell*. 2014, 13, 49–59.
4. Sisodia, S. S.; Price, D. L. Role of the beta-amyloid protein in alzheimer's disease. *Faseb. J*. 1995, 9, 366-70.
5. Jan, A.; Gokce, O.; Luthi-Carter, R.; Lashuel, H. A. The ratio of monomeric to aggregated forms of abeta40 and abeta42 is an important determinant of amyloid-beta aggregation, fibrillogenesis, and toxicity. *J.Biol.Chem*. 2008, 283, 28176-28189.

6. Tabner, B. J.; Mayes, J.; Allsop, A. D. Hypothesis: soluble aβ oligomers in association with redox-active metal ions are the optimal generators of reactive oxygen species in alzheimer's disease. *International Journal of Alzheimers Disease*. 2011,11, 546380-546380.
7. Sastre, M.; Klockgether, T.; Heneka, M. T. Contribution of inflammatory processes to alzheimer's disease: molecular mechanisms. *Int. J. Dev. Neurosci*. 2006, 24, 167-176.
8. Selvatici, R.; Marani, L.; Marino, S.,;Siniscalchi, A. In vitro mitochondrial failure and oxidative stress mimic biochemical features of alzheimer disease. *Neurochem. Int*. 2013,63, 112-20.
9. Uttara, B.; Singh, A. V.; Zamboni, P.; Mahajan, R. T. Oxidative stress and neurodegenerative diseases: a review of upstream and downstream antioxidant therapeutic options. *Curr. Neuropharmacol*. 2009,7, 65-74.
10. Wang, X.; Wang, W.; Li, L.; Perry, G.; Lee, H. G.; Zhu, X. Oxidative stress and mitochondrial dysfunction in alzheimer's disease. *Biochim. Biophys. Acta*. 2013, 1842, 1240-1247.
11. Doorn, J. A.; Petersen, D. R. Covalent adduction of nucleophilic amino acids by 4-hydroxynonenal and 4-oxononenal. *Chem. Biol. Interact*. 2003, 143-144, 93- 100.
12. Aksenov, M.Y.; Aksenova, M.V.; Butterfield, D.A.; Geddes, J.W.; Markesbery, W.R. Protein oxidation in the brain in alzheimer's disease. *Neuroscience.* 2001, 103, 373-383.
13. Athanasios, V.; Thomais, V.; Constantinos, F. 8-hydroxy-2′ -deoxyguanosine (8-ohdg): a critical biomarker of oxidative stress and carcinogenesis. *J. Environ. Sci. heal*. C. 2009,27, 120-139.
14. Swerdlow, R. H. Brain aging, alzheimer's disease, and mitochondria. *Biochim. Biophys. Acta*. 2011,1812, 1630-1639.
15. Debatin, K. M.; Poncet, D.; Kroemer, G.; Chemotherapy: targeting the mitochondrial cell death pathway. *Oncogene*. 2002, 21, 8786-803.
16. Persson, T.; Popescu, B. O.; Cedazo-Minguez, A. Oxidative stress in alzheimer's disease: why did antioxidant therapy fail. *Oxid. Med. Cell. Longev*. 2014, 427318 - 427318.
17. Racchi, M. L. Antioxidant defenses in plants with attention to prunus and citrus spp. *Antioxidants*. 2013, 2, 340-369.
18. Chen, H.; Pu, J.; Liu, D.; Yu, W.; Shao, Y.; Yang, G. Anti-inflammatory and antinociceptive properties of flavonoids from the fruits of black mulberry (morus nigral.). *Plos One*. 2016, 11, e0153080.
19. Prior, R. L.; Wu, X. Anthocyanins: structural characteristics that result in unique metabolic patterns and biological activities. *Free Radic. Res*. 2006, 40, 1014-28.
20. Kelsey, N.; Hulick, W.; Winter, A.; Ross, E.; Linseman, D. Neuroprotective effe- cts of anthocyanins on apoptosis induced by mitochondrial oxidative stress. *Nutr. Neurosci*. 2011, 14, 249-259.
21. Shukitt-Hale, B.; Cheng, V.; Joseph, J. A. Effects of blackberries on motor and cognitive function in aged rats. *Nutr. Neurosci*. 2009,12, 135-40.

22. Shih, P. H.; Chan, Y. C.; Liao, J. W.; Wang, M. F.; Yen, G. C. Antioxidant and cognitive promotion effects of anthocyanin-rich mulberry (morus atropurpurea l.) on senescence-accelerated mice and prevention of alzheimer's disease. *J. Nutr. Biochem*. 2010, 21, 598-605.
23. Butterfield, D. A.; Swomley, A. M.; Sultana, R. Amyloid β-peptide (1-42) –induced oxidative stress in alzheimer disease: importance in disease pathogenesis and progression. *Antioxid. Redox. Signal*. 2013,19, 823-35.
24. Sultana, R.; Butterfield, D. A. Oxidative modification of brain proteins in alzheimer's disease: perspective on future studies based on results of redox proteomics studies. *Journal of Alzheimers Disease Jad*. 2012, 33, S243-51.
25. Liot, G.; Bossy, B.; Lubitz, S.; Kushnareva, Y.; Sejbuk, N. Bossywetzel, E. Complex ii inhibition by 3-np causes mitochondrial fragmentation and neuronal cell death via an nmda- and ros-dependent pathway. *Cell Death Differ*. 2009, 16, 899-909.
26. Wang, X.; Perry, G.; Smith, M. A., Zhu, X. Amyloid-beta-derived diffusible ligands cause impaired axonal transport of mitochondria in neurons. *Neurodegener. Dis*. 2010, 7, 56-59.
27. Wang, X.; Su, B.; Liu, W.; He, X., Gao, Y.; Castellani, R. J. Dlp1-dependent mitochondrial fragmentation mediates 1-methyl-4-phenylpyridinium toxicity in neurons: implications for parkinson's disease. Aging Cell. 2011, 10, 807-23.
28. Kuchibhotla, K. V.; Lattarulo, C. R.; Hyman, B. T. Synchronous hyperactivity and intercellular calcium waves in astrocytes in Alzheimer mice . *Science*, 2009, 323 (5918) : 1211- 1215.
29. Kamphuis, W.; Mamber, C.; Moeton, M.; Kooijman, L.; Sluijs, J. A.; Jansen, A. H. Gfap isoforms in adult mouse brain with a focus on neurogenic astrocytes and reactive astrogliosis in mouse models of alzheimer disease. *Plos One* .2012,7, e42823.
30. Lei, W.; Zhao, Y.; Yi, L.; Akiyama, K.; Chen, C.; Qu, C. Ifn-γ and tnf-α synergistically induce mesenchymal stem cell impairment and tumorigenesis via nfκb signaling. *Stem Cells*. 2013, 31, 1383–1395.
31. Carrasquillo, M. M.; Belbin, O.; Zou, F. G.; Allen, M.; Ertekin-Taner, N.; Ansari, M. Concordant association of insulin degrading enzyme gene (ide) variants with ide mrna, abeta, and alzheimer's disease. *Plos One*. 2010, 5, e8764.
32. Jiang, Z.; Chen, C.; Xie, W.; Meng, W.; Jian, W.; Zhang, X. Anthocyanins attenuate alcohol-induced hepatic injury by inhibiting pro-inflammation signalling. *Nat. Prod. Res*. 2015, 30, 1-5.
33. Belkacemi, A.; Ramassamy, C. Anthocyanins protect sk-n-sh cells against acrolein-induced toxicity by preserving the cellular redox state. *Journal of Alzheimers Disease Jad*. 2016, 50, 981-98.
34. Badshah, H.; Kim, T. H.; Kim, M. O.; Protective effects of anthocyanins against amyloid beta-induced neurotoxicity in vivo and in vitro. *Neurochem. Int*. 2015, 80, 51–59.
35. Abdenour, B.; Charles, R. Innovative anthocyanins formulation protects neuronal-like cells

 doi:10.20944/preprints201705.0144.v1

against oxidative stress-induced damage: pharmacotherapeutic application for alzheimer's disease. *Free Radic. Biol. Med*. 2014, 75, S45.

36. Rehman, S. U.; Shah, S. A.; Ali, T.; Chung, J. I.; Kim, M. O. Anthocyanins reversed d-galactose-induced oxidative stress and neuroinflammation mediated cognitive impairment in adult rats. *Mol. Neurobiol*. 2016,1, 1-17.
37. Rabiei, Z.; Hojjati, M.; Rafieiankopaeia, M.; Alibabaei, Z. Effect of tubers ethanolic extract on learning and memory in animal model of alzheimer. *Biomedicine and Aging Pathology* .2013, 3, 185-191.

Preprints (www.preprints.org) | NOT PEER-REVIEWED | Posted: 19 May 2017 doi:10.20944/preprints201705.0144.v1

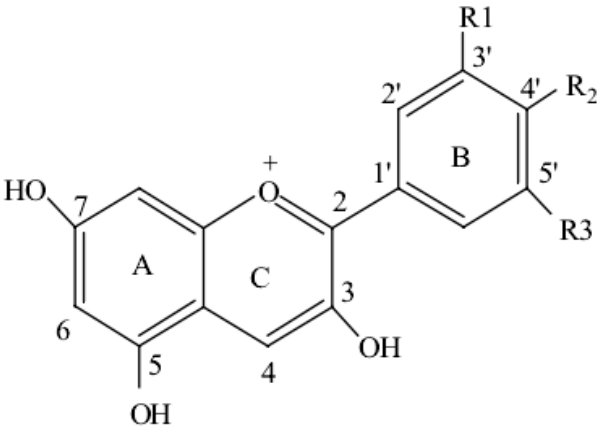

R1, R2, R3 = OH, OCH3, CH3

Fig. 1. Structure of anthocyanin.

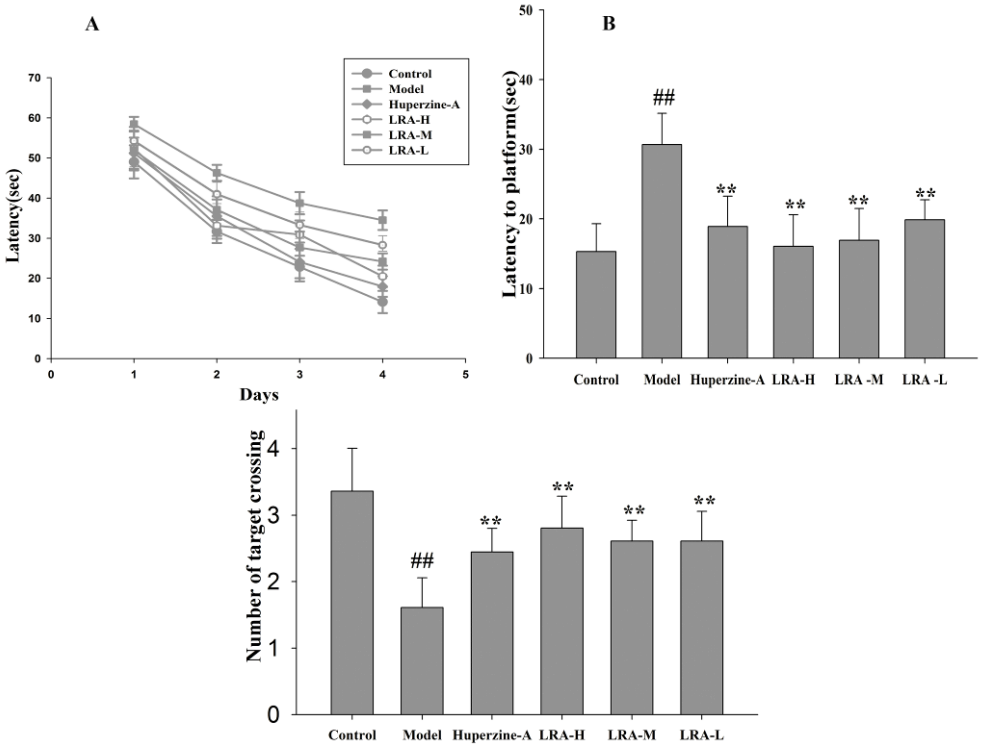

Fig. 2. Effects of LRA on rat performance in the Morris water maze test in $A\beta_{1-42}$-induced memory impairment. Morris water maze tests were employed to analyze the spatial learning and memory after 11 d of Aβ injection (n = 12). (A) Line chart of the mean escape latency time (s) during training (4 trails per day/d). (B) Comparison histogram of latencies of crossing the position where the platform was removed. (C) Comparison histogram of search frequency of crossing the target area. The data are shown as mean ± SD. Note: $^{\#}$represents significant difference ($^{\#}P < 0.05$ and $^{\#\#}P < 0.01$) from control group, *represents significant difference ($^{*}P < 0.05$ and $^{**}P < 0.01$) from $A\beta_{1-42}$-treated AD model group.

Preprints (www.preprints.org) | NOT PEER-REVIEWED | Posted: 19 May 2017 doi:10.20944/preprints201705.0144.v1

Table 1 Effects of LRA on the levels of T-SOD, CAT, GSH, MDA, and PC

Group	Dose (mg/kg)	T-SOD (U/mg protein)	CAT (U/mg protein)	GSH (mg GSH /g protein)	MDA (nmol/mg protein)	PC (nmol/mg protein)
Control	—	165.84 ± 9.68	0.51 ± 0.05	9.3 ± 0.62	1.98 ± 0.25	1.38 ± 0.37
Model	—	141.23 ± 12.40$^{\#\#}$	0.34 ± 0.03$^{\#\#}$	6.48 ± 0.64$^{\#\#}$	3.87 ± 0.40$^{\#\#}$	2.29 ± 0.26$^{\#\#}$
Huperzine-A	0.2	154.33 ± 8.60*	0.48 ± 0.06**	8.13 ± 0.74**	2.24 ± 0.27**	1.66 ± 0.50**
LRA-H	80	166.29 ± 11.98**	0.49 ± 0.06**	8.40 ± 0.47**	2.09 ± 0.27**	1.48 ± 0.38**
LRA-M	40	155.80 ± 14.89*	0.49 ± 0.05**	8.06 ± 0.59**	2.27 ± 0.29**	1.76 ± 0.31*
LRA-L	20	149.57 ± 9.95	0.40 ± 0.04*	7.39 ± 0.58*	2.37 ± 0.37**	2.08 ± 0.47

Note: $^{*}P < 0.05$ and $^{**}P < 0.01$ relative to the model group; $^{\#}P < 0.05$ and $^{\#\#}P < 0.01$ relative to the control group.

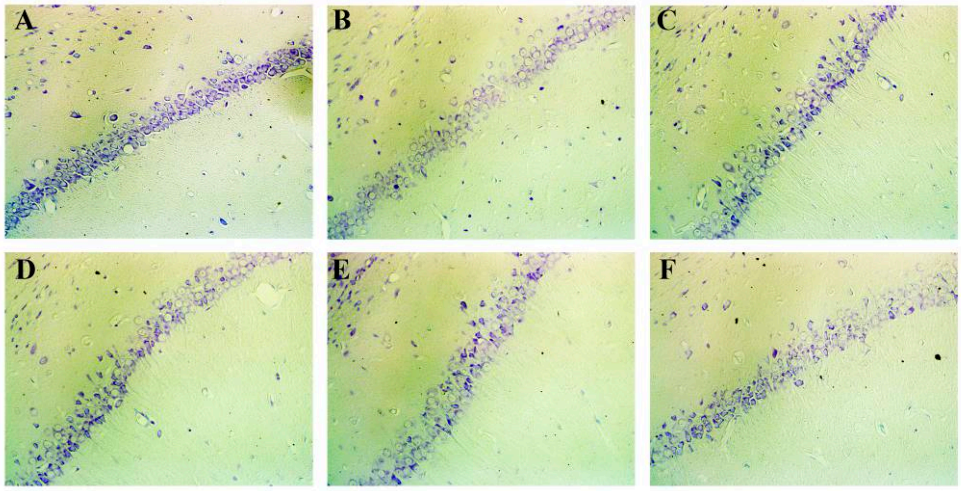

Fig. 3. Nissl staining in the CA1 region of hippocampus. Control group (A), Model group (B), Huperzine-A group (C), LRA-H group (D), LRA-M group (E), and LRA-L group (F). The photomicrographs of H&E labeling in hippocampus (400× magnification; n = 4 in each group).

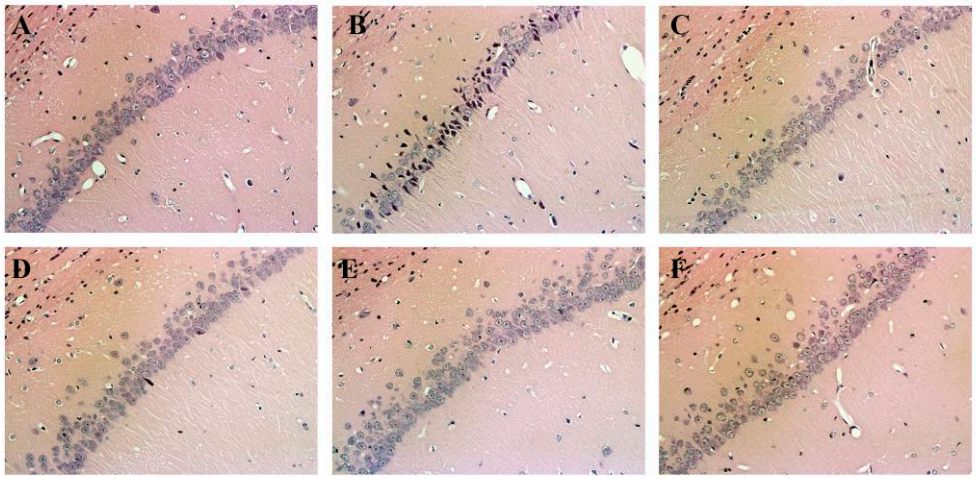

Fig. 4. Representative photomicrographs of H&E histochemical staining in the CA1 region of hippocampus for each group. Control group (A), Model group (B), Huperzine-A group (C), LRA-H group (D), LRA-M

Preprints (www.preprints.org) | NOT PEER-REVIEWED | Posted: 19 May 2017 doi:10.20944/preprints201705.0144.v1

group (E), and LRA-L group (F). The photomicrographs of H&E labeling in hippocampus (400× magnification; n = 4 in each group).

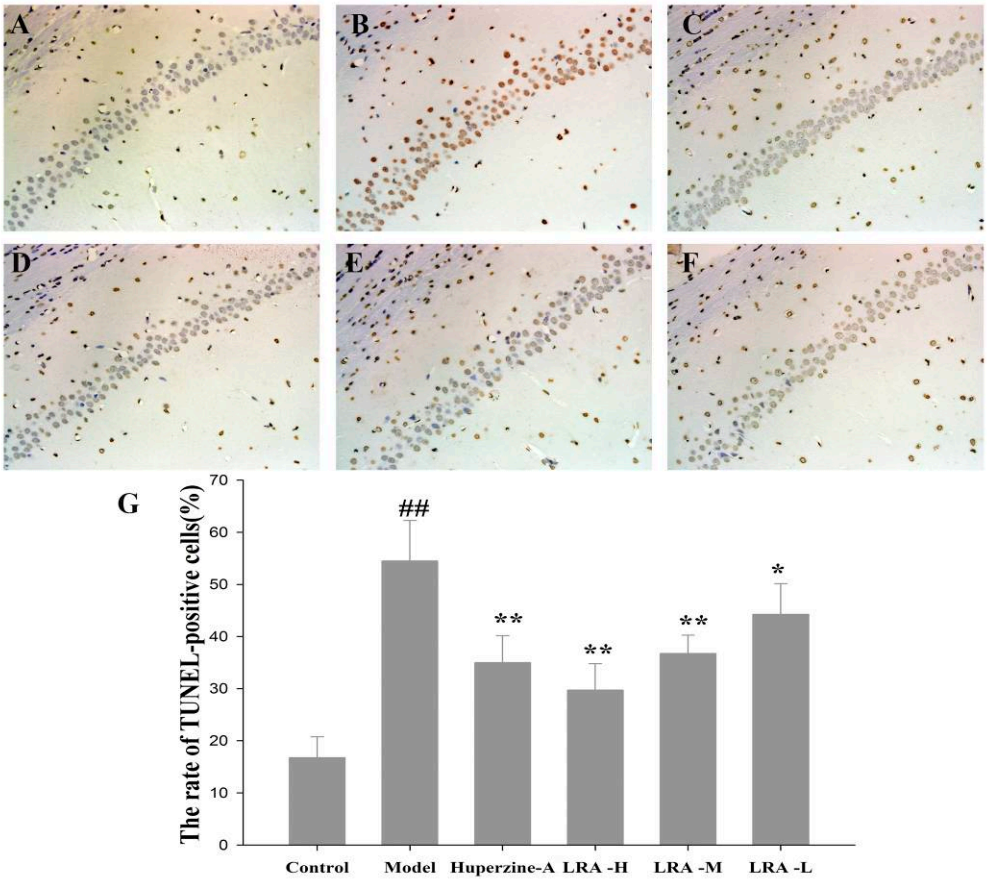

Fig. 5. Representative photomicrographs of TUNEL-positive cells for each group. Control group (A), Model group (B), Huperzine-A group (C), LRA-H group (D), LRA-M group (E), and LRA-L group (F). The photomicrographs of TUNEL labeling in hippocampus (400× magnification; n = 4 in each group). Labeling (G) is quantification of TUNEL-positive cells in each group. Data are expressed as mean ± SD (n = 4 in each group. Note: $^{\#}$represents significant difference ($^{\#}P < 0.05$ and $^{\#\#}P < 0.01$) from control group, *represents significant difference ($^{*}P < 0.05$ and $^{**}P < 0.01$) from $A\beta_{1-42}$-treated AD model group.

Preprints (www.preprints.org) | NOT PEER-REVIEWED | Posted: 19 May 2017 doi:10.20944/preprints201705.0144.v1

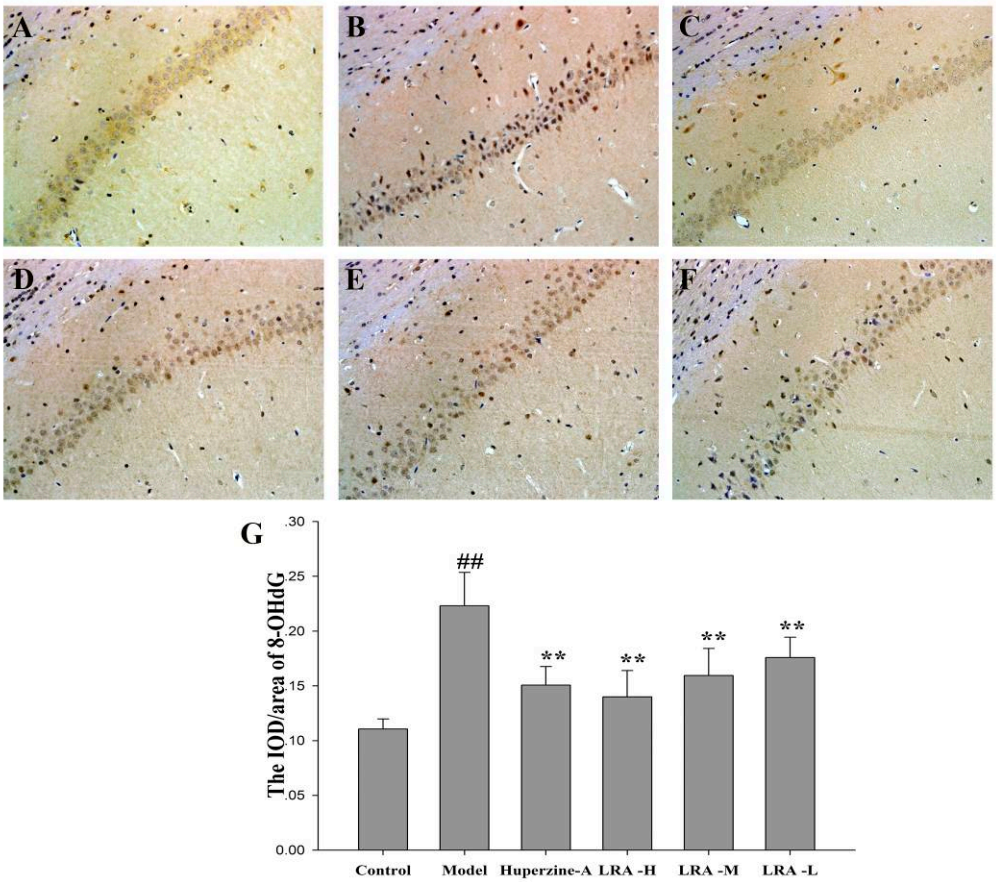

Fig. 6. Representative photomicrographs of 8-OHdG for each group. Control group (A), Model group (B), Huperzine-A group (C), LRA-H group (D), LRA-M group (E), and LRA-L group (F). The photomicrographs of 8-OHdG labeling in hippocampus (400× magnification; n = 4 in each group). (G) Quantification of 8-OHdG labeling in each group employed integral optical density (IOD)/area.Data are expressed as mean ± SD (n = 4 in each group. Note: $^{\#}$represents significant difference ($^{\#}P < 0.05$ and $^{\#\#}P < 0.01$) from control group, *represents significant difference ($^{*}P < 0.05$ and $^{**}P < 0.01$) from $A\beta_{1-42}$-treated AD model group.

Preprints (www.preprints.org) | NOT PEER-REVIEWED | Posted: 19 May 2017 doi:10.20944/preprints201705.0144.v1

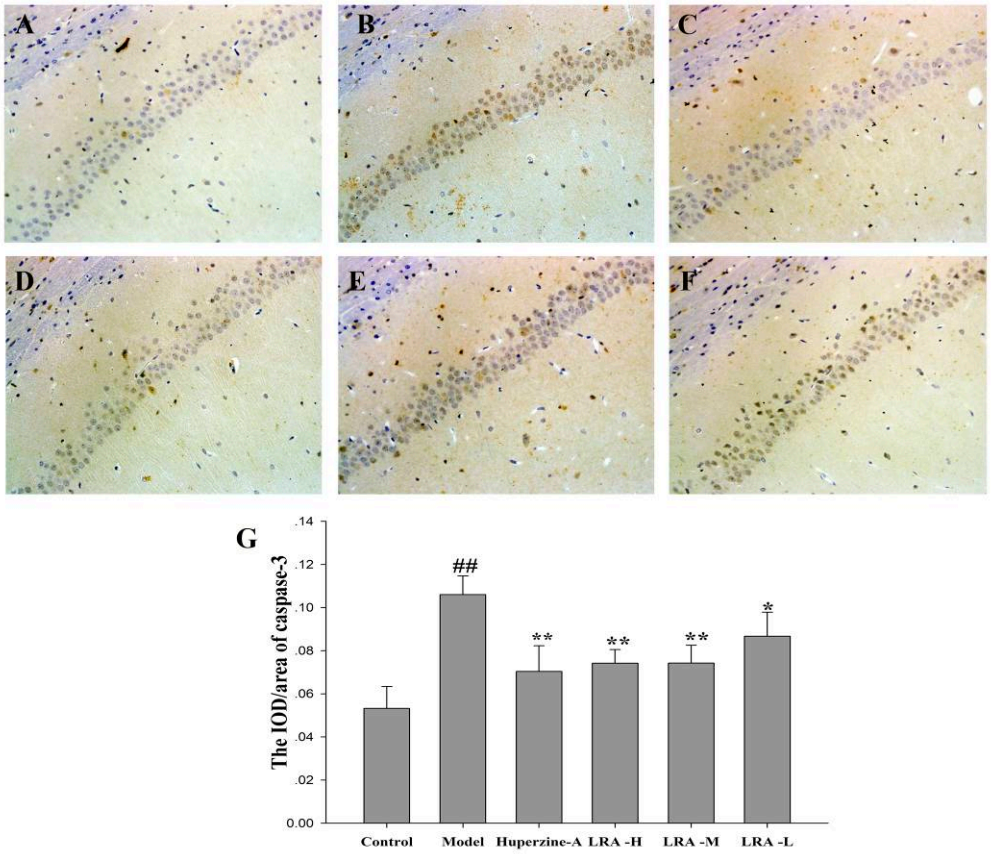

Fig. 7. Representative photomicrographs of caspase-3 for each group. Control group (A), Model group (B), Huperzine-A group (C), LRA-H group (D), LRA-M group (E), and LRA-L group (F). The photomicrographs of caspase-3 labeling in hippocampus (400× magnification; n = 4 in each group). (G) Quantification of caspase-3 labeling in each group employed integral optical density (IOD)/area. Data are expressed as mean ± SD (n = 4 in each group. Note: $^{\#}$represents significant difference ($^{\#}P < 0.05$ and $^{\#\#}P < 0.01$) from control group, *represents significant difference ($^{*}P < 0.05$ and $^{**}P < 0.01$) from $A\beta_{1-42}$-treated AD model group.

Preprints (www.preprints.org) | NOT PEER-REVIEWED | Posted: 19 May 2017 doi:10.20944/preprints201705.0144.v1

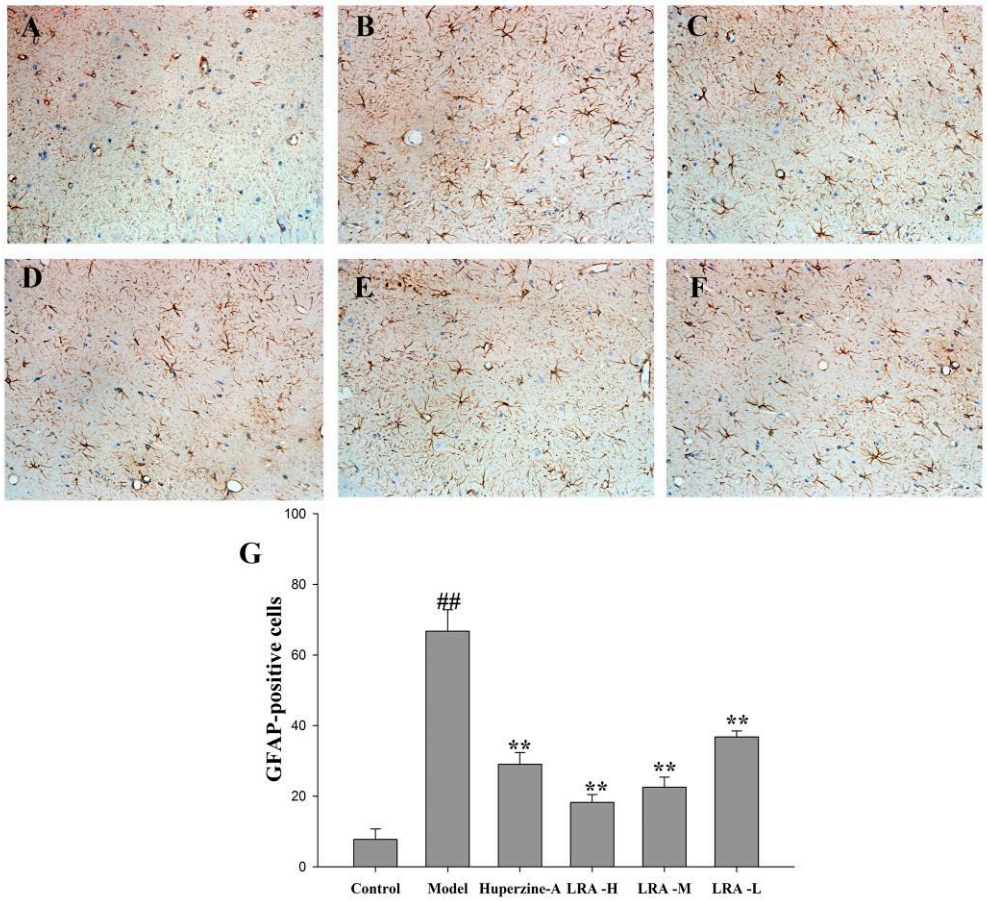

Fig. 8. Representative photomicrographs of GFAP for each group. Control group (A), Model group (B), Huperzine-A group (C), LRA-H group (D), LRA-M group (E), and LRA-L group (F). The photomicrographs of GFAP labeling in hippocampus (400× magnification; n = 4 in each group). Labelling (G) is quantification of GFAP in each group. Data are expressed as mean ± SD (n = 4 in each group. Note: $^{\#}$represents significant difference ($^{\#}P < 0.05$ and $^{\#\#}P < 0.01$) from control group, *represents significant difference ($^{*}P < 0.05$ and $^{**}P < 0.01$) from $A\beta_{1-42}$-treated AD model group.

Preprints (www.preprints.org) | NOT PEER-REVIEWED | Posted: 19 May 2017 doi:10.20944/preprints201705.0144.v1

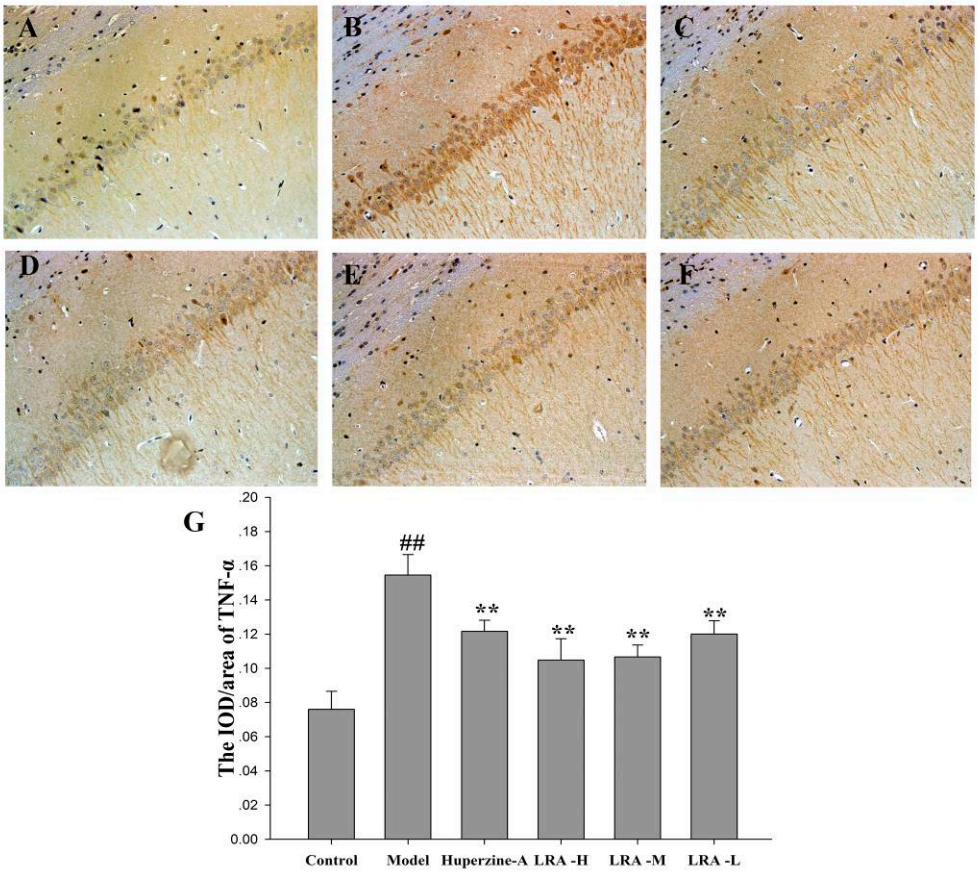

Fig. 9. Representative photomicrographs of TNF-α for each group. Control group (A), Model group (B), Huperzine-A group (C), LRA-H group (D), LRA-M group (E), and LRA-L group (F). The photomicrographs of TNF-α labeling in hippocampus (400× magnification; n = 4 in each group). (G) Quantification of caspase-3 labeling in each group employed integral optical density (IOD)/area. Data are expressed as mean ± SD (n = 4 in each group). Note: $^{\#}$represents significant difference ($^{\#}P < 0.05$ and $^{\#\#}P < 0.01$) from control group, *represents significant difference ($^{*}P < 0.05$ and $^{**}P < 0.01$) from $A\beta_{1-42}$-treated AD model group.